First-principles nonequilibrium analysis of STM-induced molecular negative-differential resistance on Si(100)

K. H. Bevan,[1,*] D. Kienle,[2] H. Guo,[3] and S. Datta[1]
[1]*NSF Network for Computational Nanotechnology, Purdue University, West Lafayette, Indiana 47907, USA*
[2]*Sandia National Laboratories, Livermore, California 94550, USA*
[3]*Centre for the Physics of Materials and Department of Physics, McGill University, Montreal, PQ, H3A 2T8, Canada*
(Received 9 January 2008; published 1 July 2008)

We report on theoretical investigations of scanning tunneling microscopy (STM)- induced molecular negative-differential resistance (NDR) on heavily *p*-type doped Si(100). Calculations are performed using the density functional theory (DFT) local density approximation (LDA) within the Keldysh nonequilibrium Green's function (NEGF) formalism. The nonequilibrium Hamiltonian is determined self-consistently for molecules on a Si(100) substrate and below a Pt(100) STM tip. We investigate in detail the nonequilibrium conditions which are likely to produce electronic *p*-type resonant NDR. The discussion is divided into two parts. First, we discuss STM distance dependence and its relation to *p*-type resonant NDR. It is shown that under high bias conditions electron tunneling is dominated by tunneling near the top of the vacuum barrier thereby preventing resonant NDR at large STM imaging distances. Second, we discuss the self-consistent bias profile and its effect on *p*-type NDR. It is shown that molecular charging effects may prevent the highest occupied molecular orbital from passing the silicon electrochemical potential, though bistable effects beyond the self-consistent NEGF-LDA method cannot be ruled out.

DOI: 10.1103/PhysRevB.78.035303 PACS number(s): 71.15.−m, 73.22.−f, 73.40.−c, 73.63.−b

I. INTRODUCTION

In recent years the scanning tunneling microscope (STM) has been increasingly applied to the characterization and construction of prototype atomic scale devices. A wide variety of STM-induced effects including radiative emission, negative-differential resistance, switching, spin flipping, and charge regulation have been observed at atomic dimensions.[1–6] Of particular technological interest, because of its complementary nature with existing silicon technology, is the observation of negative-differential resistance (NDR) in molecular STM measurements on Si(100). The conditions which give rise to electronic NDR on silicon within the ballistic regime[7] have been investigated at length in the literature both experimentally and theoretically,[6–14] and in this work we build upon existing studies to include the nonequilibrium interactions of both the scanning tunneling microscope tip and the Si(100) surface.[15] Tip-sample electronic coupling and the applied bias are both examined in detail.

To observe molecular resonant NDR with a semiconductor surface, for example silicon, it is necessary to heavily *p*-type or *n*-type dope the semiconductor to move the electrochemical potential below the valence band or above the conduction band. Under heavy *p*-type doping the electronic NDR mechanism requires a positive applied bias at the substrate to pull the highest occupied molecular orbital of a surface adsorbate past resonance at the valence band edge into the Si band gap giving rise to NDR (see Fig. 1). Conversely, the *n*-type electronic NDR mechanism requires a negative bias to pull the lowest unoccupied molecular orbital past resonance at the conduction band edge and then into the Si band gap giving rise to NDR.

Experimental investigations of resonant molecular NDR have thus far been largely limited to silicon surfaces,[8–11] where the *p*-type mechanism is believed to be due to resonant NDR and the *n*-type mechanism has had less success and is attributed to possible vibronic interactions.[12] Various molecules have been studied with reproducibility including cyclopentene,[8,9] TEMPO (Refs. 6, 9, and 11) and styrene.[6,10] The first theoretical investigation[7] of resonant molecular NDR, based on a nonorthogonal tight-binding Hückel model, explained forward and reverse bias resonant NDR asymmetry. A subsequent first-principles treatment of the device region,[12] using a simple effective mass type model for the silicon contact, yielded further insights into the nature of NDR and brought to light electrostatic considerations for

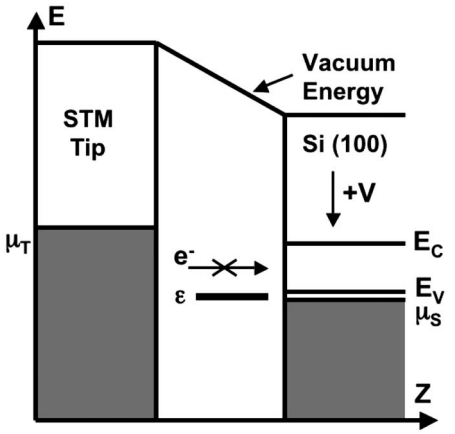

FIG. 1. Band diagram for STM-induced molecular *p*-type NDR on Si(100). A positive STM bias is applied to the substrate pulling the highest occupied molecular level, ε, past the resonance window between the Si(100) electrochemical potential, μ_S, and the valence band, E_V, into the band gap resulting in a drop in current. The current passing through ε will be orders of magnitude lower when it is inside the band gap than when it is on resonance resulting in the observed NDR.

achieving *p*-type resonant NDR. Furthermore, surface dopants, well known to be present in heavily doped silicon, were shown to play a possible role in shifting molecular levels on the substrate. Additional insights into the *p*-type NDR mechanism of cyclopentene on Si(100) were provided through GW calculations[14] in the presence of an equilibrium electric field. Both the energetic position and surface hybridization of occupied molecular states were shown to affect the interpretation of observed experimental NDR. Also, a theoretical study of negative bias (using the STM notation) NDR (Ref. 13) has shown that a reduction of tunneling at the silicon conduction band edge can give rise to NDR. There has also been some contention whether observed molecular NDR may be due to vibronic excitation of the molecule which can cause a molecule to move away from the STM tip and thereby induce NDR.[10,16] In this discussion we focus on *p*-type NDR which has been more widely studied in the literature[8,9,12,14] and do not consider vibrational effects.

We examine in detail the regime of high and low bias *p*-type NDR through a self-consistent first-principles nonequilibrium Green's function (NEGF) model including both the STM tip and Si(100) substrate atomistically. The discussion is divided into four parts where two important effects limiting *p*-type resonant NDR are presented. First, we present the atomic structure applied to this study. We have chosen styrene on Si(100) for this study since its π state is well decoupled from the Si(100) substrate,[15] which is a prerequisite for observing resonant NDR.[14] Additionally, its surface bonding properties have been well studied in the literature.[17–19] Second, we outline the transport method applied where particular attention is given to the construction of the device Hamiltonian. In the third part we analyze the STM electron transmission at various tip-sample distances and bias voltages. We show that tunneling near the top of the vacuum barrier prevents the *p*-type resonant NDR mechanism at high bias and large tip-sample distances, such that NDR should only occur at close tip-sample distances. In the fourth section we present a self-consistent density functional theory-nonequilibrium Green's function (DFT-NEGF) calculation of the tip in close contact with styrene. It is shown that the styrene π state approaches the valence band edge very slowly due to the charging energy and quantum capacitance of the molecule, thereby limiting resonant NDR [though we are unable to rule out the possibility of bistable effects beyond the self-consistent nonequilibrium Green's function-local density approximation (NEGF-LDA) method]. Lastly, we summarize our findings.

II. ATOMIC GEOMETRY

We begin by discussing the atomic geometry of our study. The system is composed of styrene on Si(100) below a Pt(100) tip [Fig. 2(b)]. The atomic structure is obtained by density functional theory (DFT) total-energy relaxation using the electronic package SIESTA.[20]

A. Tip and sample structure

To model a metal tip, we use a Pt(100)-(3×3) structure with strained coordinates to ensure that the tip geometry embeds into the (7.65 Å×7.65 Å) periodic Si(100)-(2×2) unit cell. The imposed strain on the natural Pt(100)-(3×3) unit-cell dimensions of (7.84 Å×7.84 Å) is assumed to have an insignificant effect on the metallic tip density of states (DOS) and transmission coefficient, in contrast to covalent bonded systems where bulk properties can be significantly altered, and is therefore a fair approximation which we adopt. Above silicon a 21 atom tip is placed: The first bulk-like layer is frozen and the remaining 13 tip atoms are permitted to relax.

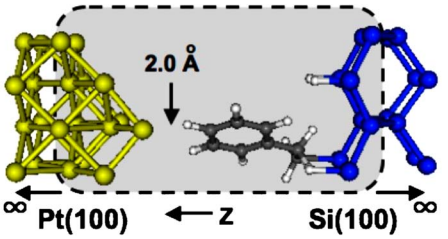

FIG. 2. (Color online) Simulated two-probe transport structure for styrene on Si(100) beneath a Pt(100) tip. The tip position of closest approach is set at 2.0 Å above the highest styrene hydrogen atom.

Styrene is known to form chains on the hydrogen passivated Si(100)-(2×1) surface.[2] The reaction is initiated at a single dangling bond and repeats by abstracting a hydrogen atom from a neighboring dimer, thereby creating a new adjacent dangling bond site, until encountering a surface defect. To reduce computation time we include only one styrene molecule in our Si(100)-(2×2) unit cell. In the STM configuration, we relax the tip above styrene at 2 Å, 4 Å, and 6 Å separations. This separation distance is defined as the distance between the highest styrene hydrogen atom and the tip apex atom. Each geometry optimization is performed via the conjugate gradient method, using the local density approximation (LDA),[20] employing a double ζ polarized basis set, and is converged to 0.01 eV/Å on a real-space grid corresponding to an energy cutoff of 300 Ryd. Relaxation calculations show that the simulated STM Pt tip physisorbs with styrene at the closest tip-sample distance of 2 Å.

The results of the relaxation are summarized at follows: The C-Si bond length is 1.89 Å, the C-C bonds within the ethylene subgroup are 1.51 Å, and the benzene ring C-C bond lengths are 1.4 Å. The angle between the C-Si bond and ethylene subgroup is 112°, the angle between the ethylene subgroup and the benzene ring is 117°, and the molecule is tilted 18° in the Si surface plane measured from the *x*-direction pointing out of the page in Fig. 2. Lastly, the molecular height above the hydrogen passivated surface is found to be 5.3 Å. We have found this geometry where the molecule leans out of the Si dimer to be 168 meV lower than the alternate configuration where the molecule leans into the Si dimer.[15,19]

B. Two-probe transport structure

Using the atomic coordinates obtained by total-energy relaxation described above, we build a two-probe transport

simulation of the tip-sample system. The two-probe system has a scattering region plus a top and a bottom lead. The scattering region consists of the atoms in the shaded box of Fig. 2. Namely, a styrene/Si(100) surface along with a 13 atom tip and two Si(100) layers are included in the scattering region. The tip is connected to a Pt lead that is modeled by perfect semi-infinite Pt(100) crystal planes extending to $z=+\infty$. Similarly, the Si substrate in the scattering region is connected to a perfect semi-infinite Si(100) lead extending to $z=-\infty$. Periodic boundary conditions are used in the transverse (x,y) directions. Lastly, a voltage bias is applied across the two leads which drives a current through the tip-sample two-probe system.

III. TRANSPORT METHOD

When a bias voltage is applied to a two-probe transport structure, the scattering region is put into a nonequilibrium state. At present, real-space DFT carried out within the Keldysh NEGF framework is the state-of-the-art technique[21–23] for analyzing nonequilibrium quantum transport through atomic systems within an *ab-initio* framework. We make use of this technique and its associated electronic package MATDCAL[21] to calculate nonequilibrium properties. The basic ideas behind the NEGF-DFT formalism are to calculate the Hamiltonian of a two-probe device system using DFT and determine the nonequilibrium quantum statistics of the transport problem using NEGF, including the electron transport open boundary conditions via real-space numerical techniques.[21,23] We briefly outline our simulation method in this section in two parts. First, we discuss the NEGF transport theory applied. Second, we discuss the procedure for calculating the device Hamiltonian at large and small tip-sample separation distances.

A. Transmission coefficient

Within NEGF, the transmission coefficient $T=T(E,V)$ is calculated via Green's functions, where E is the electron energy and V is the bias voltage. Once the DFT-NEGF single particle Hamiltonian H of the device is obtained,[21,23] the retarded Green's function G of the device scattering region at energy E is obtained as

$$G(E) = [(E + i\eta)S - H - \Sigma_S(E) - \Sigma_T(E)]^{-1}, \tag{1}$$

where η is a small positive infinitesimal and S is the overlap matrix between atomic basis functions. The quantities Σ_S and Σ_T are the self-energies of the substrate and STM tip, respectively, which account for the quantum open boundary conditions. They are calculated via recursive Fourier methods.[24,25] The transmission coefficient of a two-probe ballistic tip-sample system is determined by

$$T(E,V) = \mathrm{tr}[\Gamma_S G \Gamma_T G^\dagger], \tag{2}$$

where $\Gamma_{S,T}=i(\Sigma_{S,T}-\Sigma_{S,T}^\dagger)$ are the linewidth functions. The steady-state current under a given bias is calculated as[22]

$$I = \frac{2q}{h}\int_{-\infty}^{\infty} T(E)[f_S(E) - f_T(E)]dE, \tag{3}$$

$$f_{S,T}(E) = \frac{1}{1 + e^{(E-\mu_{S,T})/k_BT}}, \tag{4}$$

where $f_{S,T}$ is the Fermi function of the substrate/tip with an electrochemical potential of $\mu_{S,T}$. At low temperature, the integration limits reduce to the bias window, from μ_S to μ_T.

B. Device Hamiltonian

As discussed in the introduction, to induce resonant p-type NDR under bias the respective electrostatic potential must pull a level past resonance across the valence band edge into the band gap. However, the bias profile between two contacts and across a molecule is a complex effect often requiring the computationally time consuming self-consistent nonequilibrium Green's function-density functional theory (NEGF-DFT) machinery.[26] Hence, in order to obtain a first-order qualitative understanding of the potential profile, a simplistic parallel plate capacitive Laplace model is suitable (where the molecule acts as a dielectric medium). Specifically, this is valid if the STM tip is placed far away from the sample (in the weak coupling limit). In several cases it has been shown that a parallel plate capacitive Laplace model is able to adequately capture the voltage division between a STM tip and an adsorbed molecule.[8,12,15,27] This model may be simply expressed as[8,12]

$$V_{\mathrm{Mol}} = V_{\mathrm{Tot}}\left(1 + \varepsilon_{\mathrm{Mol}}\frac{Z_{\mathrm{Vac}}}{Z_{\mathrm{Mol}}}\right)^{-1}, \tag{5}$$

where V_{Mol} is the potential drop across the molecule, V_{Tot} is the potential drop across the entire system, $\varepsilon_{\mathrm{Mol}}$ is the relative molecular dielectric constant (treated as a fitting parameter), Z_{Vac} is the vacuum gap length, and Z_{Mol} is the molecular length. In this electrostatic model the single molecule is approximated by a dielectric monolayer geometry and the STM tip is assumed to behave as a flat metal plate. In the weak coupling limit, when the tip and sample are well separated, and at low bias, a Laplace capacitive model is usually valid since the molecule acts as a dielectric medium. However, when the tip is brought in close contact with the sample at high bias this approximation can fail. Therefore, we divide our transport analysis into two parts.

In our first analysis (see Sec. IV), we investigate the resonant properties of styrene through an equilibrium Hamiltonian and following Eq. (5) add in a capacitive potential drop. That is,

$$H_0 = H_{\mathrm{eq}} + V_{\mathrm{Tot}}(\vec{r}), \tag{6}$$

where $\hat{H}_{\mathrm{eq}}$ is the equilibrium tip-sample Hamiltonian at zero bias and V_{Tot} is the capacitive Laplace potential drop across the molecule and vacuum. To solve for the transmission we replace the Hamiltonian in Eq. (1) with H_0. From an analysis of barrier tunneling using the Laplace capacitive model [see Eq. (5)], we are able to show that the STM tip must be placed close to the sample in order to observe resonant NDR. In particular, it is demonstrated that the resonant tunneling current of the highest occupied molecular orbital at the valence band edge is orders of magnitude less than the contri-

bution of states tunneling near the top of the barrier at high bias and large STM tip-sample distances.

In the second part (see Sec. V), we investigate the validity of the Laplace capacitance model at close tip-sample contact and high bias. We solve for the full nonequilibrium Hamiltonian, H, through a self-consistent NEGF-DFT loop.[23] The nonequilibrium analysis reveals that an additional quantum capacitance, C_Q, must be included in the STM capacitive model. It is shown that resonant p-type NDR is impeded due to C_Q—which can be significant for atomic sized systems such as molecules—and the molecular charging energy such that the highest occupied molecular level is held fixed at the silicon electrochemical potential.

The calculation of the device Hamiltonian, both in and out of equilibrium, is carried out on a 200 Ryd real-space grid within the local density approximation. The (k_x,k_y)-space sampling is set at (4×4). The convergence criteria in the self-consistent NEGF-DFT cycle is set at 10^{-4} in both the density matrix and Hamiltonian matrix, where the Hamiltonian is stored in hartree units. We employ double ζ polarized (DZP) basis orbitals on hydrogen and carbon. For silicon and platinum a single ζ polarized (SZP) basis set is applied to all atoms. The silicon basis set is optimized, by localizing the d-orbitals,[28] to provide a bulk band gap of 1.2 eV (rather than the typical plane wave LDA band gap of 0.5 eV) with the valance band maximum located −5 eV below the vacuum level. Free atomic orbitals are placed on the top two styrene hydrogens, the uppermost styrene carbon atoms, and the Pt tip apex atom to capture the typical 1 Å/dec tunneling decay as the STM tip is pulled away from the sample.[15] Further details of the NEGF-DFT implementation can be found in Refs. 21 and 23.

IV. BARRIER TUNNELING

In this section we examine how the vacuum barrier width determines the p-type resonant NDR peak to valley ratio. The potential drop across the device for this analysis is approximated by a parallel capacitor model [see Eq. (5)]. It is shown that the peak to valley ratio decreases with increasing STM tip-sample distance. At typical STM imaging tip-sample separations high bias NDR will not be observed since the tunneling current is dominated by tunneling near the top of the vacuum barrier.[29] These results are explained through an intuitive effective barrier height model.[30]

Let us first examine the equilibrium properties of styrene on Si(100). The projected density of states (PDOS) of styrene on Si(100) is shown in Fig. 3 (as is a real-space plot of the π state orbital). From both the PDOS plot and π state wave function it is apparent that styrene presents a weakly hybridized, and therefore weakly broadened, molecular resonance. Weak hybridization, or level broadening, is a prerequisite to observe resonant p-type NDR (Ref. 14) on Si(100). Furthermore, the styrene π state is located at −6.3 eV, relatively close to the silicon valence band edge at −5 eV. Therefore from an equilibrium analysis styrene appears to be well placed for the study of resonant p-type NDR.

In STM measurements the vacuum barrier width is increased by retracting the tip away from the sample. The barrier is said to be at a minimum width when the tip is physisorbed or chemically bonded with the sample. During a STM current-voltage measurement the applied bias is split between the vacuum barrier and the molecular sample. The larger the vacuum barrier, the lesser its capacitance in relation to the molecular capacitance, and therefore the larger the fraction of the total applied bias which drops across the vacuum. At large tip-sample distances, the molecular and vacuum capacitances may be approximated roughly as parallel plate capacitors such that $C=A\epsilon/d$ (A is the area, ϵ is the dielectric constant, and d is the plate distance). As discussed earlier (see Sec. III), we determine the potential drop across the molecule and vacuum as a function of tip-sample separation by treating both the vacuum and molecule as two such parallel plate capacitors in series (see Fig. 4). In this approximation we assume that the potential drop begins at the core of the top layer of silicon atoms and ends at the tip apex atom. This can be justified by considering the metallic nature of heavily doped p-type Si(100).

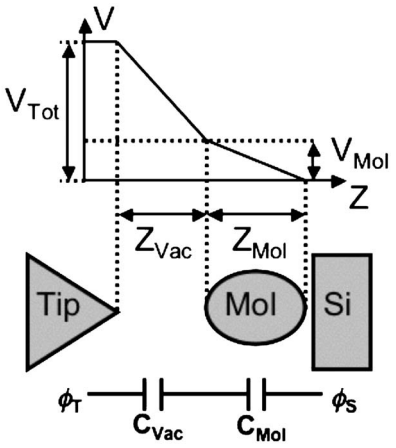

FIG. 3. PDOS for styrene on Si(100). The electrochemical potential is located at −5.2 eV. The π and π^* states are indicated. An orbital plot of the weakly hybridized π state at −6.3 eV is also shown.

The vacuum gap is approximated to be zero, $Z_{\mathrm{Vac}}=0$, when the STM tip is in full contact with styrene, that is when the highest hydrogen atom and tip apex atom are separated by 2 Å. Thus, at full contact V_{Mol} and V_{Tot} are equivalent and the applied potential is the Laplace potential. At greater STM tip-sample separations the voltage drop across the vacuum increases as determined by Eq. (5) and shown in Fig. 4. Note, $\varepsilon_{\mathrm{Mol}}$ is taken to be 2.0 for styrene following gas phase data and previous first-principles calculations.[15]

At the NDR peak bias, a resonant p-type NDR model requires that a molecular level be located between the electrochemical potential and valence band (see Fig. 1). Then as more bias is applied this level passes out of the small conduction window between the electrochemical potential and the valence band into the band gap giving rise to NDR.[7] Hence the NDR peak to valley ratio is determined by the contribution of the resonant state to the total current. If this contribution is small as is the case at high bias, then the NDR peak to valley ratio will be very small.

To determine the contribution of a molecular resonant state to the total current we can look at a transmission plot.

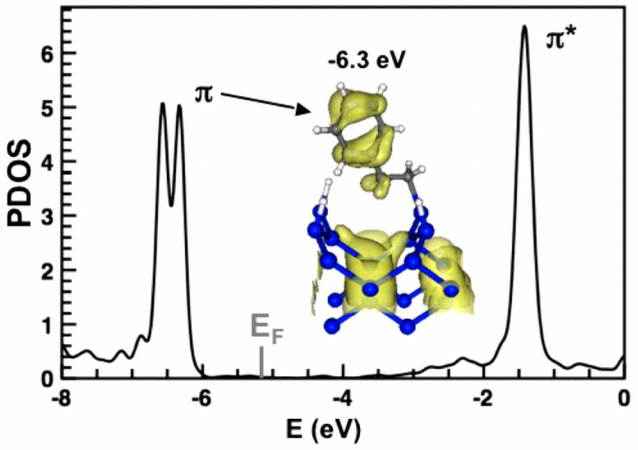

FIG. 4. (Color online) Diagram for the capacitive Laplace STM model. Parallel plate capacitances C_{Vac} and C_{Mol} are assigned to the vacuum barrier and molecule, respectively. The potential is assumed to be flat inside the metallic tip and in the heavily acceptor doped silicon substrate (for a positive STM bias). A relation between the total voltage applied, V_{Tot}, and the potential drop across the molecule, V_{Mol}, can be easily derived (Ref. 8). The tip and sample electrostatic potentials are indicated by ϕ_T and ϕ_S, respectively, where $V_{\mathrm{Tot}}=\phi_T-\phi_S$.

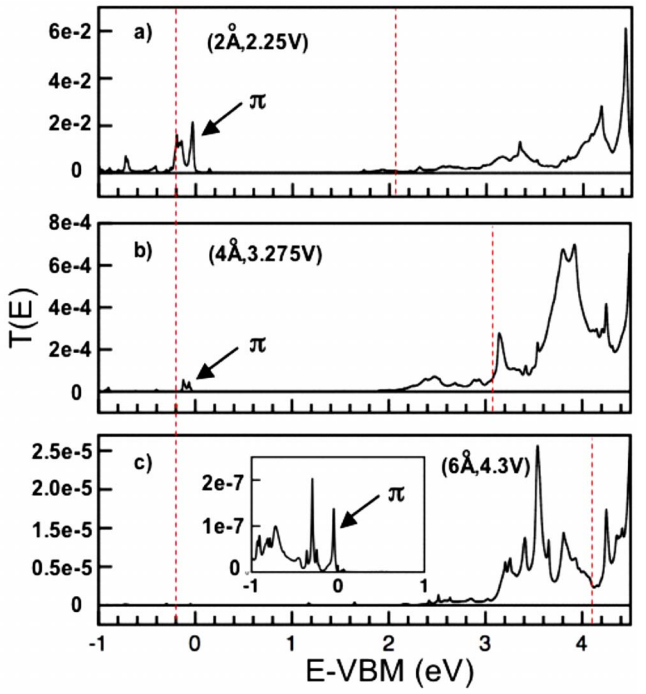

FIG. 5. (Color online) Transmission plots for styrene on Si(100) as a Pt STM tip is pulled away. The tip position of closest approach is set at a 2 Å separation between the uppermost styrene hydrogen atom and the Pt(100) tip apex atom. Transmission plots are calculated at 2 Å, 4 Å, and 6 Å separations. Zero energy is set at the silicon valence band maximum, which is located 5 eV below the bulk silicon vacuum level. The styrene π state is said to be in resonance when it lies between the silicon electrochemical potential and VBM. As the tip is pulled away more potential drops across the vacuum region and the bias at which the styrene π state is brought into resonance increases proportionally with the vacuum barrier width. The bias window is indicated by dashed red lines. The *p*-type silicon electrochemical potential assumed to lie 0.2 eV below the Si(100) valence band maximum as indicated by the leftmost dashed red line. The transmission broadening factor is 7 meV corresponding to a temperature of approximately 80 K (Ref. 8).

In Fig. 5 we plot the calculated transmission at (2 Å, 2.25 V), (4 Å, 3.275 V), and (6 Å, 4.3 V) for styrene on Si(100) beneath a Pt tip. As the tip is pulled away larger bias voltages are required to pull the styrene π state into resonance between the *p*-type silicon electrochemical potential and valence band maximum (VBM), since more voltage drops across the vacuum barrier. A noticeable effect is apparent in the transmission plots of Fig. 5: As the STM tip is pulled away the NDR peak to valley ratio decreases exponentially. The peak to valley ratio may be determined by estimating how much of the total tunneling current is contributed by the highest occupied molecular orbital at the resonance bias. NDR occurs because the tunneling current contribution of this state is lost when it is pulled into the band gap. At (2 Å, 2.25 V) we see that the resonant π state is responsible for a large fraction of conduction in the tunneling window. In Fig. 5 the tunneling window is indicated by the two dashed red lines, where the leftmost red line is the Si(100) electrochemical potential position and the rightmost red line is the Pt(100) electrochemical potential position. At (4 Å, 3.275 V) the π state transmission magnitude is diminished and is much less than the transmission near the Pt tip electrochemical potential. Therefore at a 4 Å tip-sample separation the NDR peak to valley ratio is expected to be very small. At (6 Å, 4.3 V) transmission through the π state is entirely dominated by tunneling at the Pt tip electrochemical potential. Thus, at even modest tip-sample separations the *p*-type resonant NDR magnitude could be unobservable. We term this effect NDR *washout*, where the electron tunneling rate near the top of the vacuum barrier is said to *washout* tunneling just below the silicon valence band maximum.

Though this system requires a complex first-principles model to determine molecular level motion under bias, the effect of washout can be understood in terms of a Wentzel-Kramers-Brillouin-Jeffreys (WKBJ) model. Within this model the transmission depends exponentially on the barrier width *W*,

$$T(E) \propto e^{-2/\hbar W|\sqrt{2mE}|}, \tag{7}$$

where *m* is the free-electron mass. This transmission trend is critically important to understanding observed STM tunneling *p*-type resonant NDR. The probability of tunneling at lower energies is exponentially less than at higher energies. Therefore, at high bias any contribution to the total current at low energies is washed out by tunneling at higher energies. The larger the bias, the larger the washout effect. Since an applied bias is split between the vacuum barrier and the molecule, the optimal bias for observing maximum NDR occurs at or near full tip molecule contact (thereby minimizing the washout effect).

It is important to note that although *p*-type resonant NDR has not been experimentally reported for styrene on Si(100), the effect of washout is quite general and is a property of the

tunneling barrier and not a material property of the molecule. We have chosen styrene for this analysis because it presents a weakly hybridized highest occupied molecular orbital[14] that is easily identifiable in transmission plots. However, a recent *p*-type resonant NDR study of cyclopentene on Si(100) (Ref. 8) has provided NDR measurements as a function of tip-sample separation. These results show the expected drift to high bias in the NDR peak position as the STM tip is retracted by approximately 4 Å. However, the peak magnitude does not diminish exponentially, but increases slightly, and it is likely that a nonresonant mechanism is responsible for cyclopentene NDR.[14] Furthermore, we have found through self-consistent NEGF-DFT calculations that the lowest bias cyclopentene NDR peak reported (at 2.3 V)[8] corresponds to a tip-sample vacuum gap of approximately 5.5 Å (much larger than typical physisorbtion distances of approximately 2 Å) where NDR washout is likely to be a noticeable effect.

The most important experimental implication of the washout effect is that typical STM tip-sample imaging distances,[8,10,15] of 5 Å or more, could be too distant to observe *p*-type resonant NDR. The exact tip-sample distance and voltage at which washout prevents NDR is a function of the dielectric constant and the highest occupied molecular orbital position of each individual molecule. The lower the molecular dielectric constant and the closer the highest occupied molecular level is to the valence band maximum at zero bias, the further the tip may be placed from the sample before NDR washout occurs. The precise quantitative magnitude of the washout effect depends on the WKBJ barrier height and the highest occupied molecular orbital-lowest unoccupied molecular orbital (HOMO-LUMO) energy gap of the molecule. Since LDA tends to underestimate the gap, the washout effect may be somewhat smaller than that predicted by LDA. However, in Sec. V we show that there is an even more fundamental self-consistent obstacle to resonant NDR.

This transmission study demonstrates that in order to observe *p*-type resonant NDR two criteria must be met. First, the STM tip should be physisorbed or chemically bonded with the sample to assure low bias operation and minimize direct tunneling. So far we have assumed that the potential drop follows a Laplace profile when the STM tip is physisorbed with the molecule. This assumption turns out to not be completely correct and we explore this aspect in Sec. V.

V. QUANTUM CAPACITANCE

To complete this analysis of *p*-type resonant NDR we present self-consistent NEGF-DFT calculations of the system under bias. It is shown that the styrene π state approaches the *p*-type Si(100) electrochemical potential very slowly thereby limiting resonant NDR. We explain this effect in terms of a charging energy and quantum capacitance model.

A. Styrene nonequilibrium Green's function-density functional theory bias profile

In Sec. IV it was shown that the NDR peak to valley ratio will decrease as the STM tip is pulled away from the sample.

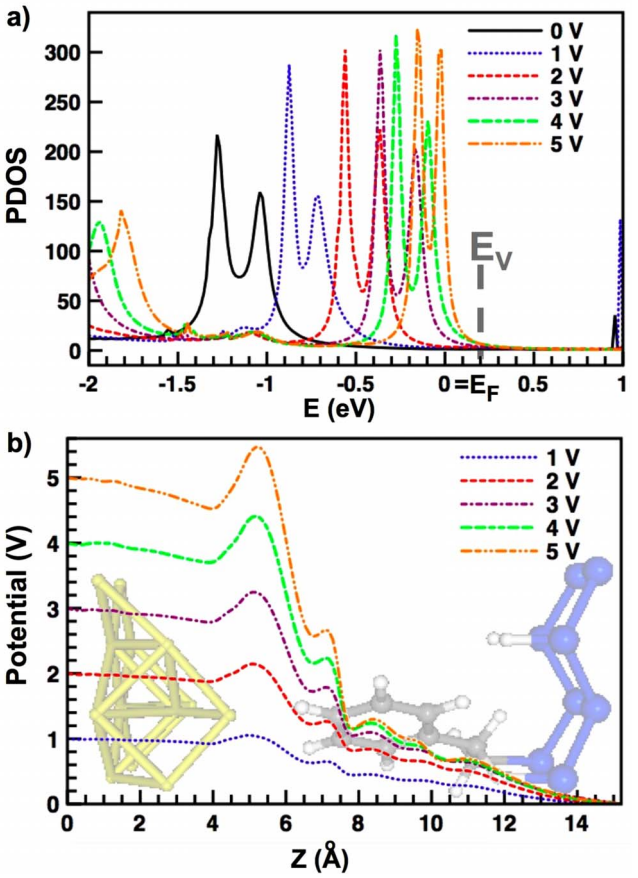

FIG. 6. (Color online) Bias characteristics of styrene attached to Si(100) in physisorbtion contact (full contact) with a Pt(100) tip. The PDOS of the styrene π state under bias is shown in (a). The potential profile across the device region is shown in (b), where a cut of the potential drop is taken through the tip apex atom. The electrochemical potential is located at −5.2 eV.

Therefore it is optimal to place a STM tip as close as possible to the molecular sample to avoid high bias operation and thus minimize NDR washout. In our NEGF-DFT analysis of styrene we therefore place the STM tip in contact with the sample and investigate its nonequilibrium properties. At full contact the distance between the tip apex atom and highest styrene hydrogen is approximately 2 Å.

Previously, in Sec. IV we assumed, within an electrostatic capacitive model, that the bias profile should approximately follow the Laplace potential when the tip is in direct contact with the styrene molecule—since the vacuum barrier is considered to have collapsed. Nonequilibrium calculations reveal an entirely different picture. In Fig. 6(a) PDOS calculations for styrene under various bias voltages ranging from 0 V to 5 V are shown. In Fig. 6(b) the same bias voltages are profiled across the device region. Each potential profile is a one-dimensional cut of the full real-space potential drop through the tip apex atom (x,y) coordinates. Two surprising features are evident in Fig. 6. First, the π state *does not pass* the Si(100) electrochemical potential even at a bias as high as 5 V. Second, the potential drop across the molecule does not follow a linear Laplace profile. Even at full contact between the STM and molecule an applied bias is split between

what remains of the vacuum gap between the tip and the molecule as seen in Fig. 6(b). At low bias the vacuum barrier between the STM tip and molecule absorbs a small fraction of the applied bias. At very high bias most of the applied potential drops across the small vacuum gap between the molecule and the STM tip.

However, contrary to intuition, below 2 V the system bias profile shown in Fig. 6(b) can be well matched by assuming a vacuum region length, Z_{Vac}, of 2 Å and a molecular region length, Z_{Mol}, of approximately 6 Å in Eq. (5)—$\varepsilon_{\mathrm{Mol}}$ is taken to be approximately 2.0. This result shows surprisingly that even when the charge densities of the tip and molecule strongly overlap, unless a chemical bond is formed, the vacuum gap cannot be considered to have collapsed from an electrostatic perspective even though it has from an electron tunneling perspective. However, the lengths of Z_{Vac} and Z_{Mol} cannot be easily justified from empirical arguments since it is not always clear where the vacuum region begins and ends at close tip-sample distances. A first-principles calculation should be conducted to validate any assumptions (especially those concerning the geometry of a system). Above 2 V the system bias profile cannot be understood purely in terms of the vacuum and molecular electrostatic capacitances (see Fig. 4). In Sec. V B 1 we show that the molecular quantum capacitance must also be included in our STM circuit model to account for the high bias behavior.

B. Styrene capacitance

In a sense we can view the high bias profile in Fig. 6(b) as a screening effect. Once the molecule begins to conduct through its highest occupied molecular orbital as shown in Fig. 6(a), a sufficient density of states is present in the bias window to screen the applied bias. Therefore at high bias, any voltage increase drops between the molecule and the metal tip. This increased screening can be understood in terms of the circuit model in Fig. 7(a) which augments the simple capacitive model of Fig. 4 with the *quantum capacitance* of the molecule as described below.

1. Quantum capacitance and electrostatic capacitance

The potential across a molecule has two contributions: a Poisson potential and a Laplace potential. The Laplace potential can be properly approximated by the series C_{Mol} and C_{Vac} capacitive model shown in Fig. 4. The Poisson potential is determined by the amount of charge gained or lost by the molecule. In the case of styrene charge is lost when the highest occupied molecular orbital is brought close to the electrochemical potential of silicon. If we change the electrochemical potential in the molecule by an amount $\delta\mu_{\mathrm{Mol}}$ and the resulting change in the electrostatic potential due to the loss of charge is $\delta\phi_{\mathrm{Mol}}$, then Poisson's equation for the molecule may be approximately written as[26]

$$\delta Q = q^2 D_o(\delta\mu_{\mathrm{Mol}} - \delta\phi_{\mathrm{Mol}}). \tag{8}$$

We define $C_Q = q^2 D_o$ to be the quantum capacitance[26,31–35] of the molecule, where q is the single electron charge and D_o is the PDOS of the molecule at μ_{Mol}. From Eq. (8) we see that the quantum capacitance serves to couple the electrostatic potential of the molecule to the electrochemical potential of the molecule.

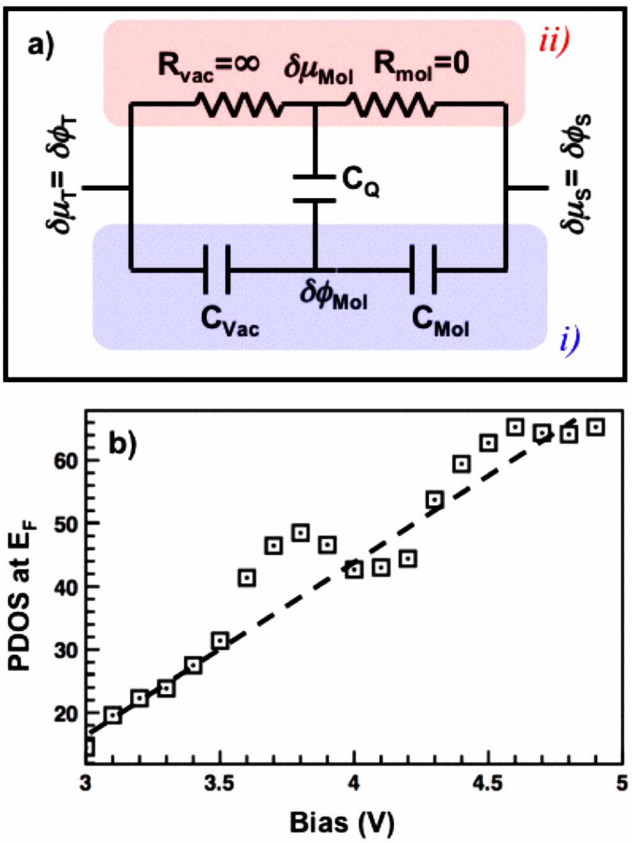

FIG. 7. (Color online) The high bias STM circuit model is shown in (a), where the quantum capacitance of the molecule couples the electrostatic potential of the molecule to the electrochemical potential of the molecule. The molecular electrochemical potential is split by the resistance of the molecule and the resistance of the vacuum barrier—see the region (ii) shaded in red. The ratio of these resistances scales exponentially with the vacuum barrier width. The original Laplace circuit model is shaded blue in region (i); this model remains valid at low bias when $C_Q \ll C_{\mathrm{Mol}}$. The ratio of C_{Vac} to C_{Mol} scales linearly with the vacuum barrier width. In subfigure (b) a plot of the PDOS of styrene at the silicon electrochemical potential as a function of applied bias for the range where the voltage drop across the molecule does not change (3–5 V) [as seen in Fig. 6(b)] is provided.

If we couple the molecule to a tip and a substrate, its electrochemical potential (μ_{Mol}) will be determined by the contact to which it is more strongly coupled. This can be understood in terms of the single-level energy dependent electron correlation function,[22]

$$G^n(E) = \frac{\gamma_S f(E-\mu_S) + \gamma_T f(E-\mu_T)}{(E-\epsilon)^2 + (\gamma_S+\gamma_T)^2/4}, \tag{9}$$

where $\gamma_{S,T}$ and $\mu_{S,T}$ are respectively the substrate and tip coupling constants and electrochemical potentials ($f(E)$ is the Fermi function). In our styrene study the substrate forms a covalent bond and the tip a physisorbtion bond, hence γ_S is greater than γ_T ($\gamma_S > \gamma_T$) and the electrochemical potential in

the molecule is determined by the Fermi distribution in the substrate.

In a circuit model we can view the molecular electrochemical potential (μ_{Mol}) as being split between the tip and substrate electrochemical potentials (μ_T and μ_S), by the vacuum resistance R_{Vac} and the molecule resistance R_{Mol} [see shaded region *ii* in Fig. 7(a)].[36] The resistances are proportional to their respective coupling constants, that is $R_{\mathrm{Vac}} \propto \gamma_S$ and $R_{\mathrm{Mol}} \propto \gamma_T$. The ratio $R_{\mathrm{Vac}}/R_{\mathrm{Mol}}$ decays exponentially as we increase the vacuum barrier width, since the tip and sample wave functions both decay exponentially into the vacuum barrier. Since the molecule couples much more strongly to the substrate than the tip, we can approximate the resistances as $R_{\mathrm{Vac}}=\infty$ and $R_{\mathrm{Mol}}=0$ [see Fig. 7(a)]. Therefore, the molecular electrochemical potential μ_{Mol} is equal to the substrate electrochemical potential μ_S and as we sweep the bias $\delta\mu_{\mathrm{Mol}}=\delta\mu_S$.

For both contacts, the change in the electrochemical potential is equivalent to the change in the electrostatic potential in the substrate, that is to say $\delta\mu_S=\delta\phi_S$ and $\delta\mu_T=\delta\phi_T$. In the Laplace picture [see Fig. 4 and shaded region *i* of Fig. 7(a)] we view the change in the molecular electrostatic potential $\delta\phi_{\mathrm{Mol}}$ to be purely a function of the molecular capacitance C_{Mol} and the vacuum capacitance C_{Vac} as we sweep the voltage bias. However, when the molecule begins to lose charge we must consider Poisson's equation and include a quantum capacitance which couples $\delta\phi_{\mathrm{Mol}}$ to $\delta\mu_{\mathrm{Mol}}$. Therefore in a circuit representation we must couple the Laplace division of the molecular electrostatic potential [$\delta\phi_{\mathrm{Mol}}$ in shaded region *i* of Fig. 7(a)] to the resistive division in the molecular electrochemical potential [$\delta\phi_{\mathrm{Mol}}$ in shaded region *ii* of Fig. 7(a)] by the quantum capacitance at a given bias (C_Q). Note, we consider the change in the electrochemical potential as we sweep the bias incrementally because the quantum capacitance (C_Q) changes with the applied bias. The circuit model of the quantum capacitance coupling between $\delta\phi_{\mathrm{Mol}}$ and $\delta\phi_{\mathrm{Mol}}$ in an STM measurement is shown in Fig. 7(a).

At low bias the quantum capacitance is very small, because the molecular density of states at the substrate electrochemical potential is very small as shown in Fig. 6(a) (we consider the low bias regime in Fig. 6 to lie below 2 V as discussed in Sec. V A). Therefore at low bias the electrochemical potential and electrostatic potential are well decoupled and the Laplace model remains valid [see Fig. 4 and shaded region *i* of Fig. 7(a)]. At high bias the molecular density of states at the substrate electrochemical potential is quite large. Thus the high bias quantum capacitance of styrene is much larger than the molecular electrostatic capacitance and the vacuum capacitance (see next paragraph). We know that C_{Vac} and C_{Mol} are comparable in size given the reasonable voltage Laplace division at 1 V in Fig. 6(b). Therefore, following Fig. 7(a), at high bias the molecular quantum capacitance dominates, tying the molecular electrostatic potential to the substrate electrochemical potential, and the most of the voltage drops across the vacuum barrier [see the bias regime above 2 V in Fig. 6(b)].

The molecular electrostatic capacitance can be roughly expressed as $C_{\mathrm{Mol}}=q^2/U_o$ where U_o is the single electron charging energy. For isolated ethylbenzene, which is styrene with two hydrogens attached similar to the passivation state of styrene on H:Si(100), the charging energy is on the order of 9 eV, thus $1/U_o \simeq 0.11\ \mathrm{eV}^{-1}$. For styrene attached to Si(100) the charging energy can be expected to reduce to a few eV due to image charge effects[37] and delocalization of the π state as it hybridizes with bulk silicon states. Whereas the styrene PDOS at the silicon electrochemical potential can be seen in Fig. 7(b) to vary between 20 eV^{-1} and 60 eV^{-1} at high bias (from 3 V to 5 V). Hence, as the highest occupied molecular orbital approaches the electrochemical potential of the substrate the molecule enters the limit of $C_Q \gg C_{\mathrm{Mol}}$ and it becomes very difficult for the level to pass the silicon electrochemical potential and NDR is prevented (since we are in the regime $\delta\phi_{\mathrm{Mol}}=\delta\mu_{\mathrm{Mol}}=\delta\mu_S$).

2. Decoupling the molecular electrochemical potential from the substrate

One could reduce the coupling to the silicon surface by inserting a large tunneling barrier between the molecule and substrate. The tunneling barrier may be composed of a vacuum region or an oxide. It should be noted, however, given the large charging energy of molecules, that the self-consistent field analysis will break down when both contacts are very weakly coupled[38] and the system will enter the Coulomb blockade regime. Furthermore, electron charging in conventional resonant tunneling diodes has been shown to produce bistability and hysteresis[39,40] and this may also be important to the operation of molecular resonant tunneling diodes.

We have found that the electrostatic and quantum capacitances together prevent the styrene π state from passing the Si(100) *p*-type electrochemical potential even when a 5 Å or 10 Å amorphous SiO_2 oxide layer[41,42] is introduced to further decouple the molecule from the substrate. Yet, we have also determined that the styrene π state delocalizes reasonably well into the SiO_2 barrier. The decay of a surface state, in this case a molecule, into an oxide layer is a material property and other oxides may better decouple the molecular states from bulk silicon than amorphous SiO_2. It has been shown that styrene can undergo desorption from *p*-type Si(100) at 1nA current levels when forward biased.[6,43] However, the introduction of an oxide layer can lower tunneling current levels down to pA and thereby significantly reduce the likelihood of desorption, which further motivates the possibility of introducing an oxide layer. A decoupling oxide layer, possessing a sufficiently low dielectric constant relative to the molecular dielectric constant, also beneficially lowers the voltage at which the highest occupied molecule orbital is brought between the *p*-type electrochemical potential and the valence band maximum.

VI. SUMMARY

We have shown that the vacuum barrier width, electrostatic capacitance, and quantum capacitance can together depreciate STM-induced *p*-type resonant NDR on Si(100). As the tip is pulled away from Si(100) less voltage drops across the molecule and the NDR peak drifts to higher voltages, since one has to apply a higher bias to shift the highest

occupied molecular orbital toward the valence band. At higher voltages the tunneling current near the top of the barrier rises exponentially and thus overwhelms tunneling through resonant occupied states. Therefore, to minimize direct tunneling (washout) it is optimal to position the STM tip as close as possible to the molecular sample, thus avoiding STM tunneling under high bias conditions. Next we examined the nonequilibrium properties of styrene on Si(100), which has a well-defined resonant π state, at bonding contact with a Pt(100) STM tip. It was shown that the electrostatic capacitance and quantum capacitance of styrene together prevent the highest occupied molecular orbital of styrene from passing the Si(100) electrochemical potential (though bistable operation beyond the self-consistent NEGF-LDA method has not been ruled out). Since charging energies and quantum capacitance effects are known to be significant for small systems, it is likely that STM-induced resonant molecular NDR could be better observed on semiconductor surfaces under ballistic conditions by further decoupling the molecule from the silicon surface via a vacuum or oxide barrier.

ACKNOWLEDGMENTS

We gratefully acknowledge financial support from NSF-NIRT and the NSF Network for Computational Nanotechnology (Purdue); NSERC of Canada, FRQNT of Quebec and CIAR (McGill). Sandia is a multiprogram laboratory operated by Sandia Corporation, a Lockheed Martin Co., for the United States Department of Energy under Contract No. DE-AC01-94-AL85000. We thank D. Waldron for his kind help with the MATDCAL software package used in this work. We also gratefully acknowledge M. C. Hersam and N. Yoder for suggesting the oxide study and many other useful discussions. We thank L. Liu for his help and expertise on SiO_2. We also thank S. Koswatta for discussions on quantum capacitance and electron charging energies.

*kbevan@purdue.edu.

[1] G. V. Nazin, X. H. Qiu, and W. Ho, Phys. Rev. Lett. **90**, 216110 (2003).
[2] P. Piva, G. A. DiLabio, J. L. Pitters, J. Zikovsky, M. Rezeq, S. Dogel, W. A. Hofer, and R. A. Wolkow, Nature (London) **435**, 658 (2005).
[3] P. Zhang, E. Tevaarwerk, B. Park, D. E. Savage, G. K. Celler, I. Knezevic, P. G. Evans, M. A. Eriksson, and M. G. Lagally, Nature (London) **439**, 703 (2006).
[4] M. Lastapis, M. Martin, D. Riedel, L. Hellner, G. Comtet, and G. Dujardin, Science **308**, 1000 (2005).
[5] A. J. Heinrich, J. A. Gupta, C. P. Lutz, and D. M. Eigler, Science **306**, 466 (2004).
[6] N. P. Guisinger, M. E. Greene, R. Basu, A. S. Baluch, and M. C. Hersam, Nano Lett. **4**, 55 (2004).
[7] T. Rakshit, G.-C. Liang, A. W. Ghosh, and S. Datta, Nano Lett. **4**, 1803 (2004).
[8] N. P. Guisinger, N. L. Yoder, and M. C. Hersam, Proc. Natl. Acad. Sci. U.S.A. **102**, 8838 (2005).
[9] N. P. Guisinger, R. Basu, M. E. Greene, A. S. Baluch, and M. C. Hersam, Nanotechnology **15**, S452 (2004).
[10] J. L. Pitters and R. A. Wolkow, Nano Lett. **6**, 390 (2006).
[11] A.-S. Hallbacka, B. Poelsemaa, and H. J. W. Zandvliet, Appl. Surf. Sci. **253**, 4066 (2007).
[12] T. Rakshit, G. C. Liang, A. W. Ghosh, M. C. Hersam, and S. Datta, Phys. Rev. B **72**, 125305 (2005).
[13] W. Lu, V. Meunier, and J. Bernholc, Phys. Rev. Lett. **95**, 206805 (2005).
[14] S. Y. Quek, J. B. Neaton, M. S. Hybertsen, E. Kaxiras, and S. G. Louie, Phys. Rev. Lett. **98**, 066807 (2007).
[15] K. H. Bevan, F. Zahid, D. Kienle, and H. Guo, Phys. Rev. B **76**, 045325 (2007).
[16] J. Gaudioso, L. J. Lauhon, and W. Ho, Phys. Rev. Lett. **85**, 1918 (2000).
[17] W. A. Hofer, A. J. Fisher, G. P. Lopinski, and R. A. Wolkow, Chem. Phys. Lett. **365**, 129 (2002).
[18] G. Kirczenow, P. G. Piva, and R. A. Wolkow, Phys. Rev. B **72**, 245306 (2005).
[19] J.-H. Cho, D.-H. Oh, and L. Kleinman, Phys. Rev. B, **65**, 081310(R) (2002).
[20] J. M. Soler, E. Artacho, J. D. Gale, A. García, J. Junquera, P. Ordejón, and D. Sánchez-Portal, J. Phys.: Condens. Matter **14**, 2745 (2002).
[21] D. Waldron, P. Haney, B. Larade, A. MacDonald, and H. Guo, Phys. Rev. Lett. **96**, 166804 (2006), and references therein.
[22] S. Datta, *Quantum Transport: Atom to Transistor* (Cambridge University Press, Cambridge, 2005).
[23] Jeremy Taylor, Hong Guo, and Jian Wang, Phys. Rev. B **63**, 245407 (2001).
[24] M. P. Lopéz Sancho, J. M. Lopéz Sancho, and J. Rubio, J. Phys. F: Met. Phys. **15**, 851 (1985).
[25] F. Zahid, M. Paulsson, and S. Datta, in *Advanced Semiconductors and Organic Nano-techniques (III)*, edited by H. Morkoc (Academic, Burlington, MA, 2003).
[26] G. C. Liang, A. W. Ghosh, M. Paulsson, and S. Datta, Phys. Rev. B **69**, 115302 (2004).
[27] R. Akiyama, T. Matsumoto, and T. Kawai, Phys. Rev. B **62**, 2034 (2000).
[28] V. I. Anisimov and A. I. Lichtenstein, in *Strong Coulomb Correlations in Electronic Structure Calculations Beyond the Local Density Approximation*, edited by V. I. Anisimov (Gordon and Breach, Amsterdam, The Netherlands, 2000).
[29] R. M. Martin, *Electronic Structure: Basic Theory and Practical Methods* (Cambridge University Press, Cambridge, 2004).
[30] C. J. Chen, *Introduction to Scanning Tunneling Microscopy* (Oxford Science, Oxford, 1993).
[31] S. Luryi, Appl. Phys. Lett. **52**, 501 (1988).
[32] M. Büttiker, J. Phys.: Condens. Matter **5**, 9361 (1993).
[33] P. Pomorski, H. Guo, R. Harris, and J. Wang, Phys. Rev. B **58**, 15393 (1998).
[34] J. Wang, H. Guo, J.-L. Mozos, C. C. Wan, G. Taraschi, and Q. Zheng, Phys. Rev. Lett. **80**, 4277 (1998).

[35] J. G. Hou, B. Wang, J. Yang, X. R. Wang, H. Q. Wang, Q. Zhu, and X. Xiao, Phys. Rev. Lett. **86**, 5321 (2001).
[36] S. Datta, W. Tian, S. Hong, R. Reifenberger, J. I. Henderson, and C. P. Kubiak, Phys. Rev. Lett. **79**, 2530 (1997).
[37] J. B. Neaton, M. S. Hybertsen, and S. G. Louie, Phys. Rev. Lett. **97**, 216405 (2006).
[38] B. Muralidharan, A. W. Ghosh, S. K. Pati, and S. Datta, IEEE Trans. Nanotechnol. **6**, 536 (2007).
[39] A. Zaslavsky, V. J. Goldman, D. C. Tsui, and J. E. Cunningham, Appl. Phys. Lett. **53**, 1408 (1988).
[40] C. A. Richter, C. A. Hacker, L. J. Richter, O. A. Kirillov, J. S. Suehle, and E. M. Vogel, Solid-State Electron. **50**, 1088 (2006).
[41] L. Liu, D. Waldron, and H. Guo, Proceedings of the Eighth International Conference on Solid-State and Integrated Circuit Technology, Shanghai, China, 23–26 October 2006, edited by Ting-Ao Tang, Guo-Ping Ru and Yu-Lnog Jiang (IEEE, New Jersey, 2006), p. 1411.
[42] Y. Tu and J. Tersoff, Phys. Rev. Lett. **84**, 4393 (2000).
[43] N. L. Yoder, N. P. Guisinger, M. C. Hersam, R. Jorn, C.-C. Kaun, and T. Seideman, Phys. Rev. Lett. **97**, 187601 (2006).